Preparation, Properties and Mechanism of Anionic and Cationic CNC/WPU Composite Films

Ya-Yu Li
Xinjiang Agricultural University https://orcid.org/0000-0003-3412-483X
Yan-Ru Bai
Xinjiang Agricultural University
Xin-Qian Zhang
Xinjiang Agricultural University
Xin Liu
Xinjiang Agricultural University
Zhen Dai
Xinjiang Agricultural University
Hong-Ji Chen
Xinjiang Agricultural University
Zun-Qi Liu (zunqi85@163.com)
Xinjiang Agricultural University
Ming-Guo Ma
Beijing Forestry University

Research Article

Keywords: Cellulose nanocrystals, Waterborne polyurethane, Microstructure, Mechanical properties, Optical properties

Posted Date: September 24th, 2021

DOI: https://doi.org/10.21203/rs.3.rs-672111/v1

Abstract

Three kinds of cellulose nanocrystals (CNCs) were added into waterborne polyurethane (WPU), and nanocomposite films were prepared by solution casting method. The influence of different ionic function groups on microstructure and properties of composite films was investigated, and interaction mechanism between these two components was analyzed. Results show that thermal stability of these composite films are improved by 15℃. Compared with sulfated CNCs （SCNCs） and TEMPO oxidized CNCs (TOCNCs), FE-SEM results prove that cationized CNCs (CaCNCs) have better dispersion in composite films. In addition, fracture surface did not display large cavities, which indicates the interface binding force between WPU and CaCNCs is stronger. The tensile strength and fracture work of CaCNC/WPU composite film increase by 11.9% and by 8.4%, respectively. The oxygen permeability of CaCNC/WPU composite film is the lowest in these composite films, which is 5.00 cm^3•cm (cm^2•s•Pa)$^{-1}$. Water vapor permeability of composite films may have a close positive correlation with their hygroscopicity. In all, composite film with CaCNCs has optimal strength, toughness, light transmittance and oxygen barrier properties. There may be opposite ion attraction superimposed hydrogen bond between CaCNCs and WPU in the composite film. The composite films are expected to have applications in food packaging, furniture coatings and biomedical applications.

Introduction

Cellulose nanocrystals (CNCs) have become the most active biomass nanoparticles in recent 20 years due to their high annual availability, renewable properties, low cost and excellent mechanical and optical properties (Foster et al. 2018). It has been investigated for tissue engineering (Sato et al. 2021), food packaging (Rader et al. 2021), optically active films (Zhang et al. 2021), and so on (Li et al. 2018).

In the previous study, we added CNCs with sulphate acid group into waterborne polyurethane (WPU) to prepare WPU/CNCs composites. It was found that CNCs had a significant enhancement on WPU films. But at the same time, elongation at break and work of fracture of these nanocomposite films were reduced exponentially (Li et al. 2020). It is generally believed that the reason is the weak interfacial force between filler and polymer matrix (Cao et al. 2007; Yu et al. 2017; Cheng et al. 2019). How to improve the interfacial compatibility between CNCs and WPU matrix and the interfacial bonding force is an urgent problem to be solved (Li et al. 2020a). At present, many methods have been reported in the literature for solving this problem. Some studies added CNCs into monomer of WPU first and then reacted between them (Cao et al. 2009; Pei et al. 2011). Weder et al. added PVA as compatibilizer between CNC and polymer matrix (Meesorn et al. 2017). Yu and Yao (Yu and Yao 2016) first prepared three kinds of CNCs with different surface functional groups, and then added them to Poly(3-hydroxybutyrate-co-3-hydroxyvalerate) (PhBV) separately. Because hydroxyl content on the surface of these three CNCs is different, the quantity of hydrogen bonds generated between CNCs and PHBV is different, too. With higher hydroxyl content, more hydrogen bonds will form. At last, the enhancement of intermolecular force will lead to improvement of tensile strength of composite film. This biodegradable composite film is expected to solve problem of white pollution and will be applied to field of food packaging. Zhao et al. (Zhao et al. 2019) prepared CNCs with different ion content and added them into ionic polymers. They found that the strength, dimensional stability and proton conductivity of composite films were all improved. These films could be used in proton exchange field.

There have been many researches focusing on enhancement of polyelectrolyte composites by using nanoparticles carrying opposite ions. For example, Usuki et al. (Usuki et al. 1993) found that ion exchange and swelling method can open the layer space of bentonite. Tang et al. prepared organic-inorganic hybrid films in light of ion crosslinking bond mechanism, via layer by layer assembly method. They showed that the composite films have strength and toughness comparable to natural shells due to sacrificing ionic bonds, which greatly promoted the process from concept to practical application (Tang et al. 2003). In 2008, Lodge (Lodge 2008) proposed concept of using ionic liquids for functional composite films preparation. Recently, Wang et al. (Wang et al. 2018b) added CNF with carboxyl to positively charged collagen fibers for composite films. The results showed that CNF improved tensile strength of the films. It can be seen that ion interaction mechanism is a very potential method for preparation of composite films (Li et al. 2016; Fan et al. 2017). Araki (Araki 2013) pointed out that surface ionization of CNCs could keep its suspension stable. However, commercially available WPUs are generally anionic WPUs. Mixing ionized CNCs with WPUs is expected to produce composites with strong interfacial forces.

Based on the above considerations, three kinds of ionized CNCs will be used in this paper, namely, Sulfated CNCs (SCNCs) prepared by sulfuric acid method, TEMPO Oxidized CNCs (TOCNCs), and Cationic CNCs (CaCNCs). These three CNCs were mixed with WPU separately, and then CNC/WPU composite films were prepared by solution casting method. Various properties of the films were systematically compared to explore the role of ion interaction mechanism in CNCs/WPU composite films.

Experimental Part

Materials

Three types of ionized CNCs are CNC produced by sulfuric acid hydrolysis method, TEMPO oxidation CNC, and cationic CNC. They are all purchased from Tianjin Woodelfbio cellulose Co., Ltd. Cotton dissolving pulp was used as raw material for CNC preparation. The information of three CNCs is shown in **Table 1**. Waterborne polyurethane (WPU, Model ADM-6161, 32.9% solid content) was kindly supplied by Shandong Audmay High Molecular Materials Co., Ltd.

As can be seen from **Table 1**, surface charge contents of these three CNCs are different. TOCNCs have the highest charge content; CaCNCs the next; SCNCs the lowest. pH of these three kinds of CNC suspension is approximately neutral. The crystallinity Index (*CrI*) of CaCNCs is slightly lower than the other two. This may be due to the fact that CNCs are cationized in alkaline solution and a small fraction of crystal transformation occurring on surface (Eyley and Thielemans 2014).

Preparation of CNC/WPU nanocomposite films

Three kinds of CNCs were taken to prepare a mixture solution of CNCs and WPU. The dry weight ratio of CNCs and WPU is 10:90. The mixture was stirred by a magnetic rotor for 30 min, and then poured into plastic petri dishes of 120 cm length. The mixture was dried at room temperature for 30 days to get nanocomposite films. These films are pure WPU, WPU-SCNCs, WPU-TOCNCs and WPU-CaCNCs films, and are coded as WC0, WSC10, WTC10 and WCC10, respectively. SC, TC and CC represent SCNCs, TOCNCs and CaCNCs, respectively. 10 represents 10 wt.% mass percentage of CNCs in the composite films. Specific compositions are shown in **Table 2**.

Table 1 Caption of three kinds of cellulose nanocrystal (CNC) suspension with different functional group

Category	Length/nm	Diameter/nm	Aspect ratio	Surface functional group	Charge density, mmol/g	Crystallinity Index	pH	Zeta potential/mV	Conductivity/ (μS/cm)	suspension concentration/(wt.%)
SCNCs	208	11	19	sulfate	0.642	90.3%	6.0-7.0	-54.2	600	1.47
TOCNCs	159	8	20	Carboxylic acid sodium	1.17	91.4%	7.0-8.0	-57.9	388	1.44
CaCNCs	196	10	20	EPTMAC	0.772	88.7%	7.0-8.0	30.4	1048	0.78

Note: SCNCs: Sulfated CNCs; TOCNCs: TEMPO Oxidized CNCs; CaCNCs: Cationized CNCs; EPTMAC: (2,3-Epoxypropyl)trimethylammonium chloride.

Table 2 Composition of WPU (WC0) and three CNC/WPU films (WSC10, WTC10 and WCC10)

Films	Mass fraction(%)			
	SCNCs	TOCNCs	CaCNCs	WPU
WC0	0	0	0	100
WSC10	10	0	0	90
WTC10	0	10	0	90
WCC10	0	0	10	90

Performance test method

Mechanical Properties

Universal mechanical testing machine (Zwick/Roell Z020, Zwick, Germany) was mounted with 200 N load force assembly. Films were cut into rectangle specimens with 10 mm wide and 40 mm long. Thickness of the specimens was measured at the central position. The film was placed between two clamps with a distance of 10.0 mm. Stretching rate was set at 5 mm/min. Five parallel samples were tested for each film composition. Mean and standard deviation values of elastic modulus, tensile strength, elongation at break and work of fracture were calculated by software.

Light transmittance

Wavelength scanning was carried out by a spectrometer (UV2310 Ⅱ, Shanghai Tianmei Scientific Instrument Co., Ltd.). The transmittance was recorded between 200 nm and 1000 nm. After that, transmittance-wavelength curves were drawn.

Surface hydrophilicity

Hydrophilicity of composite films was quantified by measuring contact angle of deionized water on the films. A microsyringe was used to drop 5 μL of deionized water onto the film. Then contact angle photos were taken using a Dynamic Contact Angle Measuring Device (SL200KS, KINO Industries, USA) equipped with a camera. The contact angle was calculated using the CAST2.0 software. Each film was measured 5 times and averaged value was adopted.

Hygroscopicity

The nanocomposite films were put into a vacuum drying oven containing anhydrous calcium chloride and dried for 24 h. Temperature was set as 50 ℃. Vacuum degree was set at 0.1 MPa. Dry weight of the nanocomposite films was gotten and was recorded as W_1 (g). A 100 mL small beaker containing 20 mL water was put in a 2 L beaker first. Then nanocomposite films were put in the 2 L beaker, outside of the 100 mL small beaker. At last, the 2 L beaker was sealed with plastic wrap and put in a 30 ℃ thermostat (ZWYR-2102C, Shanghai Zhicheng Analytical Instrument Manufacturing Co., Ltd.). This means constant temperature and humidity (30.0 ± 0.3 °C, relative humidity RH of 99± 1%) environmental conditions were setup. After 24 h, weight of the film reaching hygroscopic balance was denoted as W_2 (g). Hygroscopicity of the film is calculated as following:

$$\text{Hygroscopicity}[\%] = \frac{W_2 - W_1}{W_1} \times 100\% \quad (1)$$

Water vapor permeability

A simple experimental apparatus for measuring water vapor permeability is assembled according to method in reference (Li et al. 2020b). Nanocomposite film is mounted on the mouth of a small bottle containing anhydrous calcium chloride. Then the bottle is placed in a 2 L large beaker. After that, the 2 L large beaker is placed in a thermostat, and weight of the bottle is measured regularly. Finally, water Vapor Permeability (WVP, g•cm/(cm^2•s•Pa)) of composite film could be calculated.

Oxygen permeability

Gas permeability meter (Basic 201, Jinan Labthink Instruments Co., Ltd.) was used to test Oxygen Transmission Rate (OTR, cm^3 (cm^2·s·Pa)$^{-1}$). OTR multiplied by the thickness of nanocomposite film (cm) to get Oxygen Permeability of the thin film (OP, cm^3•cm (cm^2•s•Pa)$^{-1}$).

Structural characterization method

Fourier-transform infrared spectroscopy

FTIR spectrum of nanocomposite film was carried out on an instrument (model Nicolet 6700, Thermo Fisher Company, USA) equipped with ATR component, in the range of 600-4000 cm^{-1}, using a scanning rate of 4 cm^{-1}, and number of scans is 32 times.

Thermogravity analysis

The instrument model is 209F3(Germany Netzsch Instrument Manufacturing Co., Ltd). Weight of test samples of each film were set as 10±5 mg. Test temperature range is from room temperature to 600 ℃. Heating rate is 10 °C/min. Nitrogen flow rate is 50 mL/min.

X-ray diffraction

The instrument model is X'Pert-Pro MPD (Panalytical Corporation of the Netherlands). Cu target radiation was used (wavelength 0.154 nm, voltage 40 kV, current 40 mA). Composite film is tested while 2θ is ranging from 10° to 50°.

Field emission scanning electron microscope

A field emission scanning electron microscope (FE-SEM, model SU8010, Hitachi, Japan) was used to obtain surface and cross-sectional morphologies of the nanocomposite film. Voltage was set at 3 kV. Cross-sectional sample of film is prepared via quenching in liquid nitrogen. These samples were sprayed with gold before observation.

Results And Discussion

Chemical composition and microstructure of nanocomposite film

FTIR study

Figure 1 shows FT-IR spectra of pure WPU film (WC0) and composite films with different ionized CNCs (WSC10, WTC10 and WCC10). It can be seen that positions and intensities of most of absorption peaks of the four curves are the same. At 3332 cm^{-1}, the intensities are a little different in the four curves. This may be caused by different content of hydrogen bonds (Yu and Yao 2016). In **Figure 1(b)**, WSC10, WTC10 and WCC10 have new absorption peaks at 1161 cm^{-1}, 1110 cm^{-1}, 1059 cm^{-1}, and 1035 cm^{-1}, corresponding to the vibration peak of pyran ring of glucose in CNCs. These peaks do not appear in WC0 (Cao et al. 2007). This result indicates presence of CNCs in WSC10, WTC10 and WCC10.

Thermogravity study

Figure 2 shows thermogravimetric curves and thermogravimetric derivative curves of different nanocomposite films. When temperature is below 200°C, WPU has almost no weight loss. This indicates that the commercially available WPU has good thermal stability. Pure WPU film has two main degradation peaks. The first degradation peak is at 337 ℃, representing degradation of hard chain segment in WPU; the second degradation peak is at 375 ℃, representing degradation of the soft chain in WPU (Liu et al. 2018). When 10 wt.% various CNCs were added, the second degradation peak was increased from 375 ℃ to 390 ℃, by 15 ℃, indicating that three types of CNCs can all improve heat resistance of WPU. Yu and Yao (Yu and Yao 2016) added three kinds of CNCs with different surface hydroxyl content to PHBV matrix. It showed that the addition of CNCs increased T_{max} of PHBV by 48 ℃. This can be explained that the more hydrogen bonds formed between the CNCs and matrix, the more significantly the thermal stability of composite film is improved. Therefore, the significant improvement in the heat resistance of nanocomposite film in this work may be due to more physical and chemical interactions between three CNCs and WPU, which may be hydrogen bonds or ionic interactions.

XRD study

Figure 3 shows XRD patterns of nanocomposite films. Pure WPU film has no crystalline peaks. After adding three CNCs, diffraction peaks appeared at 2θ = 15.0°, 16.8° and 22.9°. These crystalline peaks are all characteristic peaks of cellulose I. Diffraction peak of cellulose I at 34.5° does not appear due to low content of cellulose in these films (Cao et al. 2009). However, the new diffraction peaks appearing at 29.4°, 30.7°, 39.3° and 47.4° are not characteristic peaks of cellulose. This phenomenon has not been reported in previous works (Marcovich et al. 2006; Cao et al. 2007; Wang et al. 2010; Pei et al. 2011; Victoria Hormaiztegui et al. 2016). Khan et al. (2012) prepared CNC/Chitosan nanocomposite films. XRD test showed that CNCs promoted crystallization of chitosan matrix due to the trans-crystal effect. DSC test of Santamaria-Echart et al. (2016) showed that the crystallinity of WPU increased, after 0.5% CNCs were added. Therefore, the new diffraction peaks at 29.4°, 30.7°, 39.3° and 47.4° may be caused by CNCs induced WPU crystallization.

On the other hand, Fang et al.(Fang et al. 2014) found two weak diffraction peaks at 18° and 42° 2θ in XRD pattern of PU. They think these two peaks should be the characteristics of soft segments PPG in polyurethane. If we know the molecular structure of WPU here, the recognition of new diffraction peaks would be easy. However, the WPU in this work was supplied by a company and we do not know its ingredients entirely. The diffraction peaks of PU at 27.8° and 29.2° 2θ were only reported by Zhang et al. (Zhang et al. 2012); after addition of modified CNC, the intensities of these peaks increased; to our disappointment, Zhang et al.(2012) did not supply the structure of PU, too. This black box about molecular structure of WPU makes the huge difficulty to confirm the new XRD peaks. Moreover, the intensity 29.4° 2θ was weak and at the same order of magnitude of the amorphous peak at 19.0° 2θ of WC0. In addition, the new XRD peaks are considerably sharper, and start at a higher 2θ value, than might be expected for a polymer. So another possibility is that the new XRD peaks at around 29.4°, 30.7°, 39.3° and 47.4° 2θ are ascribed to a few impurities.

In all, we need more information to confirm the new XRD peaks.

SEM study

Figure 4 is SEM photographs of surface of different nanocomposite films. It can be seen that the surface of film WC0 is very flat and dense; the surface of film WTC10 appears micron-dimension (**Figure 4-WTC10-1**) and nano-dimension (**Figure 4- WTC10-3**) cracks; these cracks indicate that compatibility between WPU and TOCNCs is very poor. The surface of film WSC10 is relatively flat and dense, but with some linear protrusions. These protrusions are dispersed CNCs, indicating that compatibility between WPU and SCNCs is good. The surface of film WCC10 is smooth and dense, also with some linear protrusions. These protrusions are also dispersed CNCs, indicating that compatibility between WPU and CaCNCs is also very good.

Figure 5 is cross-sectional SEM photographs of different nanocomposite films. The cross-section of pure WPU film WC0 only has micron-dimension flaky exfoliation. At nano-size, its cross section is very flat (**Figure 5-WC0-3**). The cross-sections of three nanocomposite films are relatively rough in micron size (scaler 20μm, **XXX-1**). Among them, the cross section of WTC10 is most rough, while WCC10 is little rough. There are some TOCNCs agglomerates of about 1 μm size in WTC10 (photo **WTC10-2**), which can be explained as an island-like distribution of TOCNCs in matrix. Photo **WTC10-2** also confirms that roughness on photo **WTC10-1** is caused by CNCs agglomerates. Pei et al. (Pei et al. 2010) also observed SCNCs agglomerates of about 1 μm.

In photo **WTC10-3** of **Fig. 5**, a cavity with diameter of about 200 nm was found (red dotted line). It can be inferred that this cavity was produced due to the pulling out of agglomerate. This phenomenon also proves that the interface force between WPU and TOCNCs is poor. Some cavities were also observed in WSC10 but smaller, about 100 nm (red and blue dotted line, photo **WSC10-3**). However, no distinct cavity was found in WCC10 (photo **WCC10-3**).

According to the pullout mechanism of material fracture (Munch et al. 2008), these observation support that the interface binding force between WPU and CaCNCs is stronger. When CNCs have electric charge of same character as the WPU matrix, the CNCs tend to agglomerate into small patches due to electrostatic repulsion between CNCs and WPU. The formation of small patches will also be driven by the formation of hydrogen bonds between CNCs. Because TOCNCs carry about twice the negative charge of SCNCs, TOCNCs are easier to agglomerate than SCNCs. Pei et al. (Pei et al. 2010) improved compatibility between CNCs and PLLA matrix through hydrophobic modification; finally CNCs were dispersed uniformly in the matrix. Li et al. (Li et al. 2016) prepared CNCs with positive charges but different concentrations on its surface first; then added them to matrix carboxymethyl cellulose; along with surface charge of CNCs gradually increased, SEM results showed that CNCs dispersed more and more uniformly in the matrix. The authors believes that this is due to electrostatic repulsion between CNCs of the same charge. Similar to the principle of "*dissolution in the material of similar structure*", charging of CNCs can also improve their dispersion in polymer matrix, and result in stronger electrostatic interaction between molecules with different charges, at the same time. Finally, a composite film with better performance could be obtained.

Marcovich et al. (Marcovich et al. 2006) and Cao et al. (Cao et al. 2009) pointed out that the cross-section of nanocomposite film containing CNCs had dots. They assumed that these dots are cross-sections of CNCs. In XXX-3 of **Figure 5** (the scale is 200nm), there are dot-like protrusions on the cross-sections of WSC10 and WCC10 (red dotted triangles). They should be also cross-sections of single CNCs exposed. This also supports that the dispersion of CNCs in films WSC10 and WCC10 is better than that in film WTC10.

Performance of nanocomposite films

Mechanical performance

Figure 6(a) shows the stress-strain curves of different nanocomposite films. The information of elastic modulus, tensile strength, elongation at break and work of fracture were extracted from these stress-strain curves, and the average values and standard deviation were calculated to make histograms, as shown in **Figure 6(b-e)**. It can be seen from **Figure 6(b)** that after adding three CNCs, the elastic modulus of all 3 composite films were improved, and the composite film added with SCNCs increased most of all, that is 71.3%. It can be seen from **Figure 6(c)** that tensile strength of the composite film added with SCNCs and TOCNCs decreased, and tensile strength of the composite film added with TOCNCs decreased most of all, while the composite film added with CaCNCs improved, with an increase of 11.9%. It can be seen from **Figure 6(d)** that elongation at break of composite films added with three CNCs decreased, and that of the composite film added with SCNCs decreased most of all, by 42.8%; the elongation at break of composite film added with TOCNCs decreased moderately, by 34.5%; the elongation at break of composite film added with CaCNCs decreased least of all, by 11.1%. It can be seen from **Figure 6(e)** that work of fracture of composite films added with SCNCs and TOCNCs decreased. Work of fracture of the composite film added with TOCNCs decreased most of all, by 26.7%, while that of the composite film added with CaCNCs increased by 8.4%. Li et al. (Li et al. 2019) added chitosan and copper ions into CNFs; tensile strength and elastic modulus of the prepared composite films were increased by 104% and 75%, respectively. What is even more impressive is that compared with pure CNFs film, toughness of the composite film increased by 560%. The authors believe that this is the result of dual effects of hydrogen bonding and ion coordination among the three components in composites.

On the whole, the composite film with CaCNCs has the best strength and toughness. The CaCNCs in WCC10 composite film are evenly dispersed in the matrix and have the best interface compatibility with matrix. This is consistent with the SEM characterization results.

Appearance and UV-vis spectra study

Figure 7 is a photograph of appearance of different nanocomposite films. These composite films have a smooth surface and good light transmittance. Among them, pure WPU film has the best light transmittance. But there are some wrinkles on its surface. Composite film with TOCNCs has the worst light transmittance. **Figure 8** shows the UV-vis spectra of different nanocomposite films. After three CNCs are added, the light transmittance of composite films decreases. Among them, the light transmittance of composite film with TOCNCs decreases most. This is because TOCNCs are unevenly distributed in the film, and the film surface has many micron-sized and nano-sized cracks. This phenomenon is also observed in SEM photographs in **Figure 4**. The light transmittance of composite film with CaCNCs is highest among 3 composite films, which is consistent with good compatibility of the two components and densest structure observed in SEM of **Figure 5** (Yano et al. 2005; Girouard et al. 2016).

The result of **Fig. 8** is also consistent with **Fig. 7**. Girouard et al. (Girouard et al. 2016) blended modified and unmodified CNCs with PU to prepare films. Results showed that modification changed the appearance of film from white to transparent. The authors explored reasons for the change in appearance of films and believed that this was due to the uniformly dispersed CNCs in PU matrix after modification.

Surface hydrophilicity study

Table 3 shows contact angles of different nanocomposite films. By taking pure WPU film as a control, contact angle of nanocomposite films decreased due to addition of CNCs. This is because CNCs themselves contain a large number of hydroxyl groups, which have strong hydrophilicity and enhance hydrophilicity of films. Among them, hydrophilicity of WTC10 film increased the most. This is because there are many cracks on the surface of WTC10 film. Water droplets are easily immersed in rough surface (Liu et al. 2017). Hydrophilicity of WCC10 film is lower than WTC10 film. Hydrophilicity of WSC10 film is the lowest. This may be due to the higher charge content and lower crystallinity of CaCNCs, compared to SCNCs (Aulin et al. 2009).

Table 3 Contact angle of WPU (WC0) and CNC/WPU films (WSC10, WTC10 and WCC10) with three kinds of CNCs

Films	WC0	WSC10	WTC10	WCC10
Contact angle/°	83.0	74.3	28.1	64.4

Hygroscopicity and water vapor permeability study

Figure 9 shows the hygroscopicity of different nanocomposite films. It can be seen that hygroscopicity of film with cationic CNCs is the largest. This may be due to that CaCNCs have lowest crystallinity and are most easily swelled by water vapor among the three types of CNCs (Aulin et al. 2009).

Figure 9 also shows water vapor permeability (WVP) of different nanocomposite films. The WVP of composite film with SCNCs decreased; but WVP of composite film with TOCNCs increased slightly, and WVP of composite film with CaCNCs increased significantly. This is consistent with slight increase of hygroscopicity of WPU/TOCNC composite film and a large increase of hygroscopicity of WPU/CaCNC composite film. Therefore, WVP of composite film may have a close positive correlation with its hygroscopicity. Kumar et al. (Kumar et al. 2014) reached the same conclusion. Wang et al. (Wang et al. 2018a) also analyzed some parameters for the mechanism of WVP change of composite films containing nanocellulose. They carried out detailed investigations on three films of cellulose pure film, cellulose coated film and cellulose reinforced film. Results showed that barrier properties of cellulose to water vapor is relatively poor. To achieving good water vapor barrier properties, materials with low WVP coefficient such as polyethylene should be used with nanocellulose to form a sandwich structure. Compared with the currently widely used synthetic plastics, this multilayer composite material has great competitive potential in the packaging materials market.

Oxygen permeability study

Figure 10 shows the oxygen permeability (OP) of different nanocomposite films. It can be seen that after adding three kinds of ionized CNCs, the OP of films decreases greatly. This is because CNCs are highly crystalline nanoparticles, and their addition can make oxygen transmission path tortuous. Among these 3 nanocomposite films, the oxygen permeability of film with cationic CNCs is the lowest, 5.00 cm^3•cm $(cm^2$•s•Pa$)^{-1}$, which is 34.4% lower than the control film. This may be due to that the structure of composite film with cationic CNCs is denser than the others. So the existence of CaCNCs makes the path of oxygen passing through film more tortuous than that of other CNCs (Wang et al. 2018a). Compared with composite films WSC10 and WCC10, OP of WTC10 film is slightly higher. This may be caused by the uneven distribution of TOCNCs in the film. Because of uneven distribution of TOCNCs in the film, the local area with a low concentration of nanoparticles will become a channel for oxygen permeation (Wang et al. 2018b).

Conclusions

Three CNC/WPU composite films consisting of water-based polyurethane (WPU) and three different ionized cellulose nanocrystals (CNCs) were prepared by casting method. Compared with pure WPU control sample, thermal stability of composite films is increased by 15 ℃. FE-SEM results showed that cationized CNCs (CaCNCs) are uniformly distributed in matrix, and the composite film structure is dense. Tensile strength of composite film with CaCNCs increased by 11.9%, and work of fracture increased by 8.4%, which are all optimal values of the three composite films. Composite film with CaCNCs has the highest optical transmittance, too. After adding three kinds of ionized CNCs, the oxygen permeability (OP) of films decreased greatly, and the OP value of film with CaCNCs decreased most, by 34.4%. Comprehensive performance of CaCNC/WPU composite film is best of all. The mechanism may be: CaCNCs are nanoparticles with cations, while WPU is a polymer emulsion with anions; there are opposite ion attraction and superimposed hydrogen bonding between them. This components interaction ultimately makes structure of composite film compact. The prepared composite material is expected to find applications in food packaging, furniture coatings and biomedicine.

Declarations

Acknowledgments This work was supported by the research program of National Natural Science Foundation of China (No. 21561030 and No. 51863021).

Author contributions All authors contributed to the study conception and design. Material preparation, data collection and analysis were performed by Ya-Yu Li, Yan-Ru Bai and Ming-Guo Ma. The first draft of the manuscript was written by Ya-Yu Li and Zun-Qi Liu commented on previous versions of the manuscript. All authors read and approved the final manuscript.

Conflicts of interest The authors declare no conflicts of interest.

Availability of data and material Not applicable

Code availability Not applicable

References

1. Araki J (2013) Electrostatic or steric? - preparations and characterizations of well-dispersed systems containing rod-like nanowhiskers of crystalline polysaccharides. Soft Matter 9: 4125-4141. http://doi.org/10.1039/c3sm27514k.
2. Aulin C, Ahola S, Josefsson P, Nishino T, Hirose Y, Osterberg M, Wagberg L (2009) Nanoscale cellulose films with different crystallinities and mesostructures-their surface properties and interaction with water. Langmuir 25: 7675-7685. http://doi.org/10.1021/la900323n.
3. Cao XD, Dong H, Li CM (2007) New nanocomposite materials reinforced with flax cellulose nanocrystals in waterborne polyurethane. Biomacromolecules 8: 899-904. http://doi.org/10.1021/bm0610368.
4. Cao XD, Habibi Y, Lucia LA (2009) One-pot polymerization, surface grafting, and processing of waterborne polyurethane-cellulose nanocrystal nanocomposites. Journal of Materials Chemistry 19: 7137-7145. http://doi.org/10.1039/b910517d.
5. Cheng G, Zhou M, Wei Y-J, Cheng F, Zhu P-X (2019) Comparison of mechanical reinforcement effects of cellulose nanocrystal, cellulose nanofiber, and microfibrillated cellulose in starch composites. Polymer Composites 40: E365-E372. http://doi.org/10.1002/pc.24685.
6. Eyley S, Thielemans W (2014) Surface modification of cellulose nanocrystals. Nanoscale 6: 7764-7779. http://doi.org/10.1039/c4nr01756k.
7. Fan J, Li T, Ren YZ, Qian XR, Wang QW, Shen J, Ni YH (2017) Interaction between two oppositely charged starches in an aqueous medium containing suspended mineral particles as a basis for the generation of cellulose-compatible composites. Industrial Crops and Products 97: 417-424.

http://doi.org/10.1016/j.indcrop.2016.12.048.

8. Foster EJ, Moon RJ, Agarwal UP, Bortner MJ, Bras J, Camarero-Espinosa S, Chan KJ, Clift MJD, Cranston ED, Eichhorn SJ, Fox DM, Hamad WY, Heux L, Jean B, Korey M, Nieh W, Ong KJ, Reid MS, Renneckar S, Roberts R, Shatkin JA, Simonsen J, Stinson-Bagby K, Wanasekara N, Youngblood J (2018) Current characterization methods for cellulose nanomaterials. Chem. Soc. Rev. 47: 2609-2679. http://doi.org/10.1039/c6cs00895j.
9. Girouard NM, Xu SH, Schueneman GT, Shofner ML, Meredith JC (2016) Site-selective modification of cellulose nanocrystals with isophorone diisocyanate and formation of polyurethane-CNC composites. ACS Appl. Mater. Interfaces 8: 1458-1467. http://doi.org/10.1021/acsami.5b10723.
10. Khan A, Khan RA, Salmieri S, Le Tien C, Riedl B, Bouchard J, Chauve G, Tan V, Kamal MR, Lacroix M (2012) Mechanical and barrier properties of nanocrystalline cellulose reinforced chitosan based nanocomposite films. Carbohydr. Polym. 90: 1601-1608. http://doi.org/10.1016/j.carbpol.2012.07.037.
11. Kumar V, Bollstrom R, Yang A, Chen QX, Chen G, Salminen P, Bousfield D, Toivakka M (2014) Comparison of nano- and microfibrillated cellulose films. Cellulose 21: 3443-3456. http://doi.org/10.1007/s10570-014-0357-5.
12. Li MC, Mei CT, Xu XW, Lee S, Wu QL (2016) Cationic surface modification of cellulose nanocrystals: Toward tailoring dispersion and interface in carboxymethyl cellulose films. Polymer 107: 200-210. http://doi.org/10.1016/j.polymer.2016.11.022.
13. Li YY, Wang B, Ma MG, Wang B (2018) Review of recent development on preparation, properties, and applications of cellulose-based functional materials. International Journal of Polymer Science 10: 1-19. http://doi.org/10.1155/2018/8973643.
14. Li T, Zhang X, Lacey SD, Mi R, Zhao X, Jiang F, Song J, Liu Z, Chen G, Dai J, Yao Y, Das S, Yang R, Briber RM, Hu L (2019) Cellulose ionic conductors with high differential thermal voltage for low-grade heat harvesting. Nature Materials 18: 608-613. http://doi.org/10.1038/s41563-019-0315-6.
15. Li S F, Wen XN, Ju WL, Su YL, Wang DJ (2020a) Effects of particle-polymer interactions and particle-particle interactions on mechanical properties of polymer nanocomposites. Acta Polymerica Sinica, 52: 1-12. http://doi.org/10.11777/j.issn1000-3304.2020.20189.
16. Li YY, Jing WW, Wang JH, Li JF (2020b) Elucidating the relationship between structure and property of WPU-CNCs nanocomposite films. Sci. Adv. Mater. 12: 1213-1224. http://doi.org/10.1166/sam.2020.3767.
17. Liu M, Wang S, Jiang L (2017) Nature-inspired superwettability systems. Nat. Rev. Mater. 2: 1-17. http://doi.org/10.1038/natrevmats.2017.36.
18. Liu ZM, Wu B, Jiang YY, Lei JX, Zhou CL, Zhang JH, Wang JL (2018) Solvent-free and self-catalysis synthesis and properties of waterborne polyurethane. Polymer 143: 129-136. http://doi.org/10.1016/j.polymer.2018.04.010.
19. Lodge TP (2008) Materials science - a unique platform for materials design. Science 321: 50-51. http://doi.org/10.1126/science.1159652.
20. Marcovich NE, Auad ML, Bellesi NE, Nutt SR, Aranguren MI (2006) Cellulose micro/nanocrystals reinforced polyurethane. J. Mater. Res. 21: 870-881. http://doi.org/10.1557/jmr.2006.0105.
21. Meesorn W, Shirole A, Vanhecke D, de Espinosa LM, Weder C (2017) A simple and versatile strategy to improve the mechanical properties of polymer nanocomposites with cellulose nanocrystals. Macromolecules 50: 2364-2374. http://doi.org/10.1021/acs.macromol.6b02629.
22. Munch E, Launey ME, Alsem DH, Saiz E, Tomsia AP, Ritchie RO (2008) Tough, bio-inspired hybrid materials. Science 322: 1516-1520. http://doi.org/10.1126/science.1164865.
23. Pei AH, Zhou Q, Berglund LA (2010) Functionalized cellulose nanocrystals as biobased nucleation agents in poly(l-lactide) (PLLA) - crystallization and mechanical property effects. Compos. Sci. Technol. 70: 815-821. http://doi.org/10.1016/j.compscitech.2010.01.018.
24. Pei AH, Malho JM, Ruokolainen J, Zhou Q, Berglund LA (2011) Strong nanocomposite reinforcement effects in polyurethane elastomer with low volume fraction of cellulose nanocrystals. Macromolecules 44: 4422-4427. http://doi.org/10.1021/ma200318k.
25. Rader C, Weder C, Marti R (2021) Biobased polyester-amide/cellulose nanocrystal nanocomposites for food packaging. Macromolecular Materials and Engineering 306. http://doi.org/10.1002/mame.202000668.
26. Santamaria-Echart A, Ugarte L, Garcia-Astrain C, Arbelaiz A, Angeles Corcuera M, Eceiza A (2016) Cellulose nanocrystals reinforced environmentally-friendly waterborne polyurethane nanocomposites. Carbohydr. Polym. 151: 1203-1209. http://doi.org/10.1016/j.carbpol.2016.06.069.
27. Sato R, Arita T, Shimada R, Nohara T, Tabata K, Koseki K, Umemoto K, Masuhara A (2021) Biocompatible composite of cellulose nanocrystal and hydroxyapatite with large mechanical strength. Cellulose 28: 871-879. http://doi.org/10.1007/s10570-020-03550-7.
28. Tang Z, Kotov NA, Magonov S, Ozturk B (2003) Nanostructured artificial nacre. Nature Materials 2: 413. http://doi.org/10.1038/nmat906
29. Usuki A, Kojima Y, Kawasumi M, Okada A, Fukushima Y, Kurauchi T, Kamigaito O (1993) Synthesis of nylon 6-clay hybrid. J. Mater. Res. 8: 1179-1184. http://doi.org/10.1557/JMR.1993.1179.
30. Victoria Hormaiztegui ME, Lujan Mucci V, Santamaria-Echart A, Angeles Corcuera M, Eceiza A, Ines Aranguren M (2016) Waterborne polyurethane nanocomposites based on vegetable oil and microfibrillated cellulose. Journal of Applied Polymer Science 133: article number: 44207. http://doi.org/10.1002/app.44207.
31. Wang YX, Tian HF, Zhang LN (2010) Role of starch nanocrystals and cellulose whiskers in synergistic reinforcement of waterborne polyurethane. Carbohydr. Polym. 80: 665-671. http://doi.org/10.1016/j.carbpol.2009.10.043.
32. Wang JW, Gardner DJ, Stark NM, Bousfield DW, Tajvidi M, Cai ZY (2018a) Moisture and oxygen barrier properties of cellulose nanomaterial-based films. ACS Sustainable Chemistry & Engineering 6: 49-70. http://doi.org/10.1021/acssuschemeng.7b03523.
33. Wang WH, Zhang XL, Li C, Du GH, Zhang HJ, Ni YH (2018b) Using carboxylated cellulose nanofibers to enhance mechanical and barrier properties of collagen fiber film by electrostatic interaction. J. Sci. Food Agric. 98: 3089-3097. http://doi.org/10.1002/jsfa.8809.
34. Yano H, Sugiyama J, Nakagaito AN, Nogi M, Matsuura T, Hikita M, Handa K (2005) Optically transparent composites reinforced with networks of bacterial nanofibers. Advanced Materials 17: 153-155. http://doi.org/10.1002/adma.200400597.

35. Yu HY, Yao JM (2016) Reinforcing properties of bacterial polyester with different cellulose nanocrystals via modulating hydrogen bonds. Compos. Sci. Technol. 136: 53-60. http://doi.org/10.1016/j.compscitech.2016.10.004.
36. Yu HY, Zhang H, Song ML, Zhou Y, Yao J, Ni QQ (2017) From cellulose nanospheres, nanorods to nanofibers: Various aspect ratio induced nucleation/reinforcing effects on polylactic acid for robust-barrier food packaging. ACS Appl. Mater. Interfaces 9: 43920-43938. http://doi.org/10.1021/acsami.7b09102.
37. Zhang FS, Zheng XT, Wang CL, Wang DD, Xue XY, Qing GY (2021) Synthesis of optically active chiral mesoporous molybdenum carbide film. Journal of Industrial and Engineering Chemistry 94: 482-488. http://doi.org/10.1016/j.jiec.2020.11.023.
38. Zhao Q, Wei YC, Ni CJ, Wang LL, Liu BJ, Liu J, Zhang MY, Men YF, Sun ZY, Xie HM, Hu W, Lu YF (2019) Effect of aminated nanocrystal cellulose on proton conductivity and dimensional stability of proton exchange membranes. Applied Surface Science 466: 691-702. http://doi.org/10.1016/j.apsusc.2018.10.063.

Figures

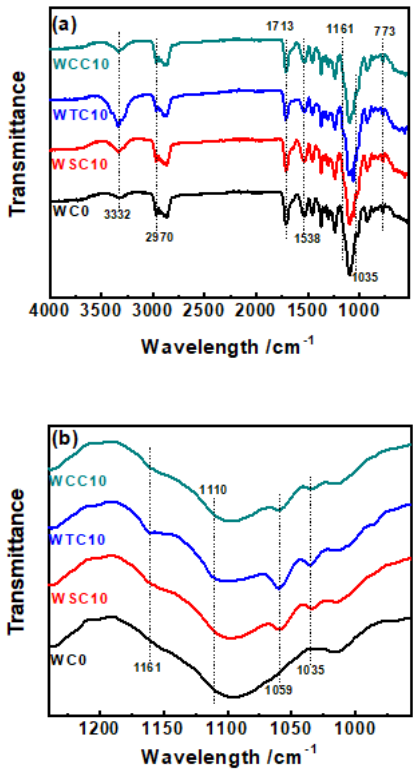

Figure 1

FT-IR spectra of pure waterborne polyurethane (WPU) (WC0) and CNCs/WPU films (WSC10, WTC10 and WCC10) with three kinds of CNCs

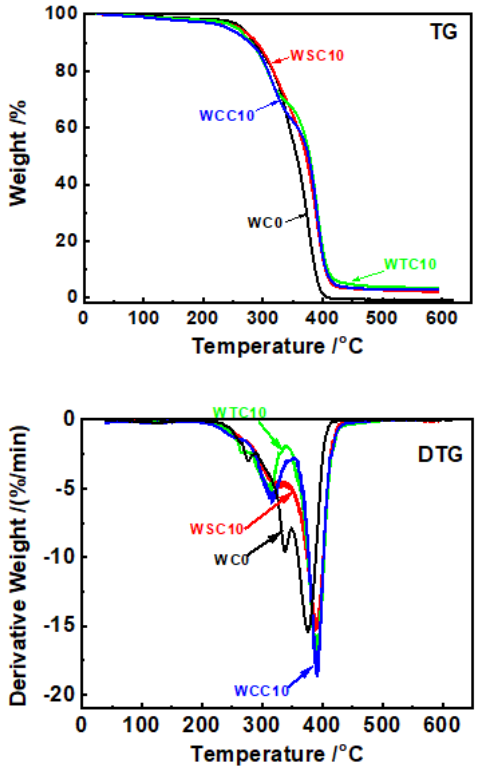

Figure 2

Thermal-gravimetric (TG) and derivative thermal-gravimetric (DTG) curves of WPU (WC0) and CNCs/WPU films (WSC10, WTC10 and WCC10) with three kinds of CNCs

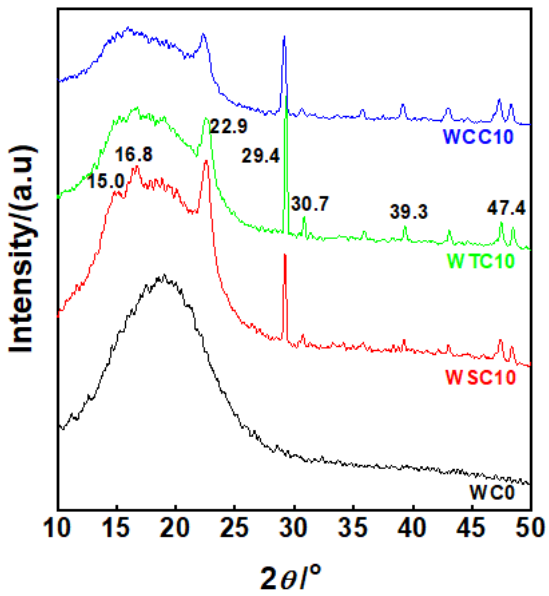

Figure 3

XRD patterns of WPU (WC0) and CNCs/WPU films (WSC10, WTC10 and WCC10) with three kinds of CNCs

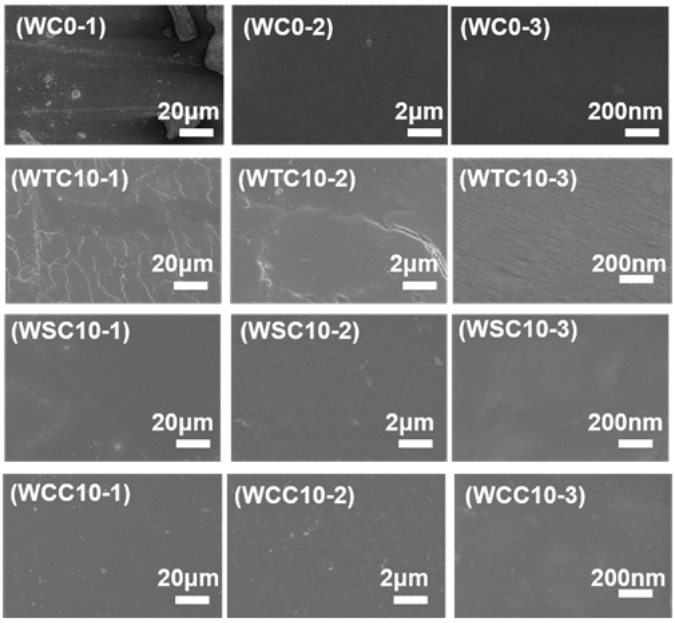

Figure 4

FE-SEM micrographs of surface of WPU (WC0) and CNCs/WPU films (WTC10, WSC10 and WCC10) with three kinds of CNCs

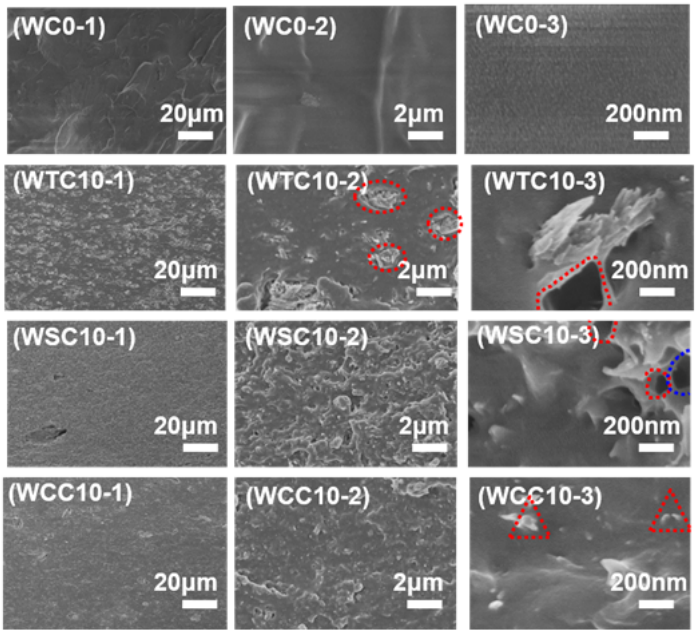

Figure 5

FE-SEM micrographs of cross section of WPU (WC0) and CNCs/WPU films (WTC10, WSC10 and WCC10) with three kinds of CNCs

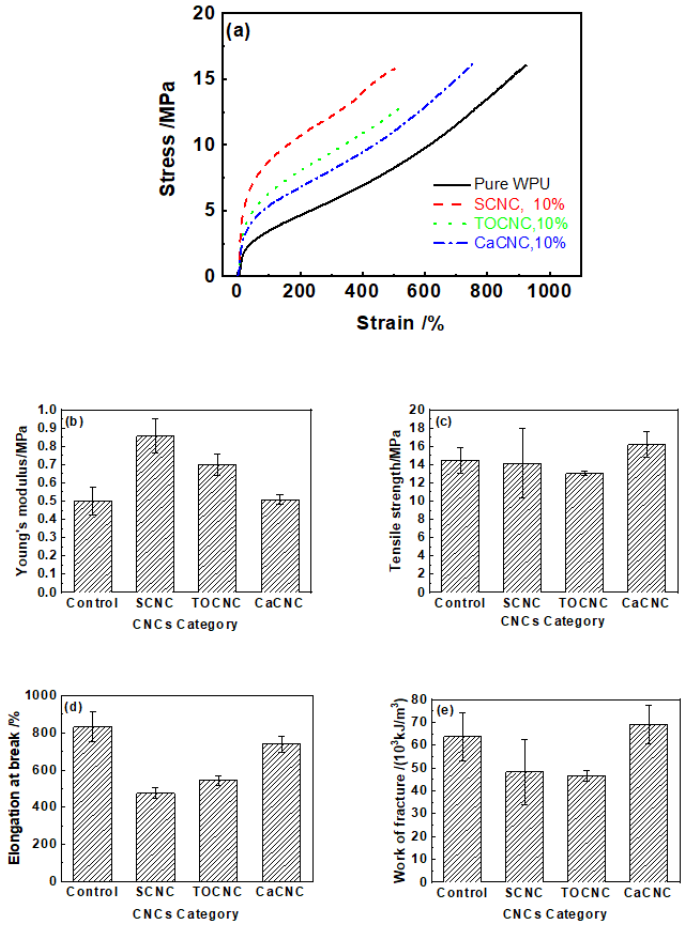

Figure 6

Typical stress-strain curves (a), Young's modulus (b), tensile strength (c), elongation at break (d), and work of fracture (e) of WPU (control) and CNCs/WPU films with three kinds of CNCs (The CNCs category was marked in figure. The CNCs content is 10 wt.% in all 3 composite films)

Figure 7

The appearance pictures of WPU (WC0) and CNCs/WPU films (WTC10, WSC10 and WCC10) with three kinds of CNCs

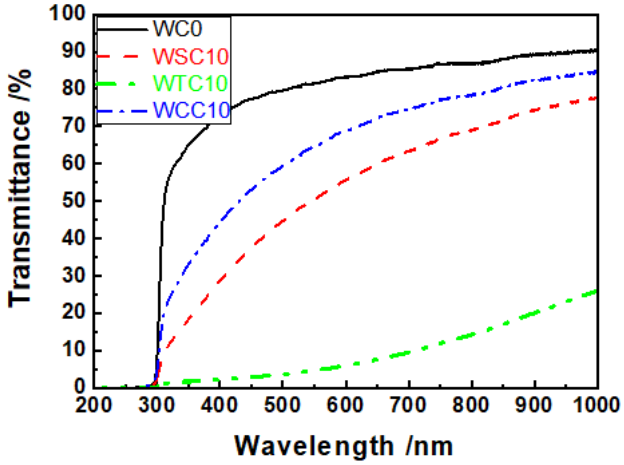

Figure 8

The UV-vis spectra of WPU (WC0) and WPU-CNCs films (WSC10, WTC10 and WCC10) with three kinds of CNCs

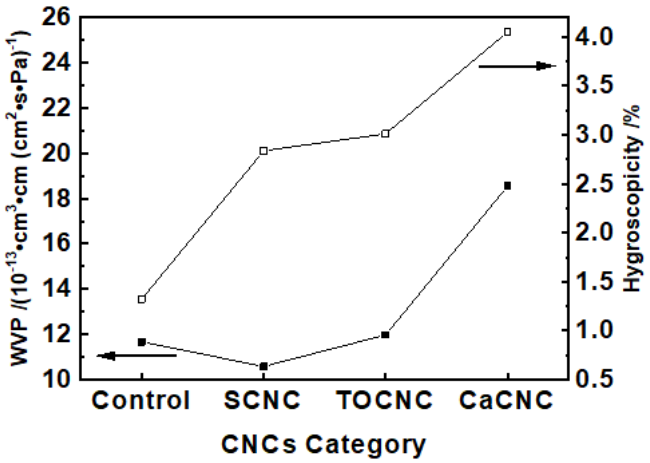

Figure 9

Hygroscopicity and WVP of WPU and WPU-CNCs films with three kinds of CNCs (The CNCs category was marked in figure. The CNCs content is 10 wt.% in all 3 composite films)

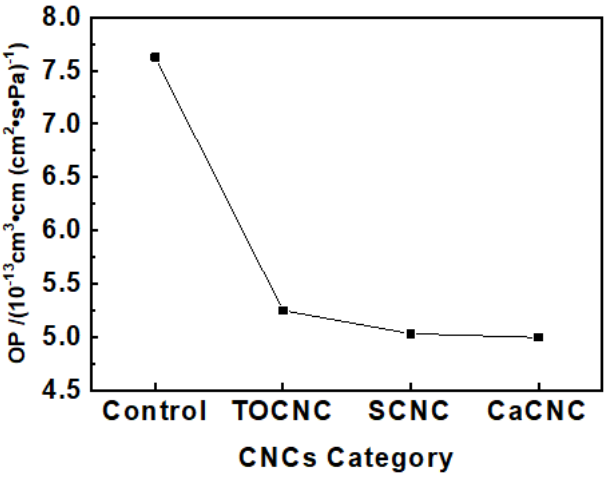

Figure 10

The OP of WPU and CNCs/WPU films with three kinds of CNCs (The CNCs category was marked in figure. CNCs content is 10 wt.% in all 3 composite films)

Supplementary Files

This is a list of supplementary files associated with this preprint. Click to download.

- graphicabstract.docx
- SupplementaryInformation1.docx